Supporting Information:

Enhancing Scanning Electrochemical Microscopy's Potential to Probe Dynamic Co-Culture Systems *via* Hyperspectral Assisted-Imaging

Sondrica Goines[a], Mingchu Deng[a], Matthew W. Glasscott[a†], Justin W. C. Leung[b], and Jeffrey E. Dick[a,c*]

[a]Department of Chemistry, The University of North Carolina at Chapel Hill, Chapel Hill, NC 27599, USA

[b]Department of Radiation Oncology, College of Medicine, University of Arkansas for Medical Sciences, Little Rock, AR 72205, USA

[c]Lineberger Comprehensive Cancer Center, The University of North Carolina at Chapel Hill, Chapel Hill, NC 27599, USA

Corresponding author: jedick@email.unc.edu

Table of Contents **Page**

Hyperspectral Motivation

Two technical approaches to studying biological interactions are: 1) genomics and 2) single-cell biology. While genomics uncovers heterogeneities over a large number of cells, it often masks biological interactions at the single-cell level.[1] Optical microscopy is commonly used to assess cell viability based on cell morphology. [2] While this technique constitutes a simple means of analysis, conventional microscopy techniques, such as bright field microscopy, offer limited optical data. For example, within bright field images, one typically cannot discern between a single cell and a cell undergoing proliferation. Additional information may be acquired through the use of fluorescence probes in live cell imaging.

A robust means to studying biological interactions within two-dimensional cell cultures is the use of fluorescence microscopy, but to uncover dynamic changes with respect to paracrine or intercellular interactions, one must use multiple fluorescence probes or focus on analytes with known spectral properties.[1, 3, 4] Fluorescence microscopy allows one to track the activity of fluorescently-tagged cellular organoids or biomolecules at a probe-specific wavelength. Furthermore, fluorescent probes have increased the spatial resolution of live cell imaging within biological systems research.[5, 6] Unfortunately, fluorescence microscopy is limited to the use of standard filter cubes, which only allow a user to excite or measure a range of wavelengths. As the field of live cell microscopy continues to develop, new techniques such as hyperspectral imaging, are necessary to widen the scope of research. Furthermore, the use of tunable filters in hyperspectral imaging has allowed users to increase spectral discrimination in comparison to the use of standard gratings.

Spectral imaging combines the use of optical microscopy and spectroscopy to obtain spatial and spectral information from each pixel of an image.[3, 4, 7] NASA initially introduced spectral imaging systems to study temperature and weather patterns, but such systems have been broadly developed for bioanalytical research[4]; for example, spectral imaging has been used to understand pharmacological responses[4], single-cell viability[8, 9], and carcinogenesis[9-13]. While most methods depend on labeling the analyte of interest, others have used spectral imaging to characterize analytes with known spectral properties, such as the experimental drug doxorubicin with known fluorescence properties.[4] Specifically, hyperspectral imaging allows one to take a series of images over time at various excitation or emission wavelengths that results in a lambda stack of images. This series of images is combined to provide a hyperspectral image in which a spectrum can be

obtained at each pixel of the image.[14] Spectral resolution is dependent on the diffraction gratings, integrated prisms, or filter cubes used by a spectral detector within the optical system.[14, 15]

Hyperspectral imaging is often achieved when high resolution confocal microscopy is paired with time lapse imaging; within these systems tunable filters are used to discriminate between fluorophores within a sample.[7] Confocal microscopy is favored over conventional optical techniques for fluorescence imaging because it offers sufficient lateral resolution to reduce background fluorescence as well as optical axial resolution.[16-18] For spectral imaging, filter cubes within confocal systems are scanned to separate fluorophores based on a lambda stack acquired during a time lapse.[7] Here, a white light laser illumination source would be ideal, as it produces all wavelengths within the visible spectrum. Though white light laser confocal microscopy and bright field microscopy have been used to acquire hyperspectral images of nanoparticles smaller than tens of nanometers, the high cost of the laser is a deterrent compared to conventional systems.[19, 20] The system presented in this manuscript permits the acquisition of hyperspectral images at marketable cost.

Hyperspectral imaging is commonly used within nanomaterials research as a means to image single metal nanoparticles based on their surface plasmon resonance.[21-24] Paired with complementary electrochemical techniques, hyperspectral systems may be used to optically resolve and study electrochemical systems.[21, 24, 25] When applied to biological systems, hyperspectral imaging techniques can be used as a means to track cellular interactions. Though some have developed label-free methods of hyperspectral imaging, such as hyperspectral imaging based on resonant technology, most rely on fluorescence.[10, 23, 26] By combining hyperspectral imaging with electrochemical techniques, researchers have developed methods to quantitatively study redox reactions of single entities in real time.[21, 24, 27] Development of a cost efficient system that allows this quantitative analysis is the goal of this work.

Our hyperspectral assisted-biological scanning electrochemical imaging platform widens the scope of biological imaging by allowing the user to capture correlated optical, electrochemical, and spectral data simultaneously. Additionally, our variable fluorescence bandpass source, characterized by a xenon illumination source coupled to a Sutter Instrument® two-stage Lambda VF-5™ tunable filter changer**,** allows a user to capture standard fluorescence images in bypass mode as well as spectral data with 1 nm wavelength resolution rather than a limited wavelength range as achieved when using standard filter cubes. Our tunable excitation filters have a dynamic

range of 380 nm to 620 nm, while our tunable emission filters have a range of 440 nm to 700 nm. To obtain a fluorescence image, an excitation wavelength is directed through an inverted microscope using a VF-5^{TM} tunable filter changer, while a second tunable filter changer is used to select wavelength-specific emitted photons to be collected by an adjacent digital camera. By specifying an excitation wavelength while scanning a series of emission wavelengths, we may obtain a set of hyperspectral images in which an emission spectrum can be recorded for each individual pixel within a frame. Alternatively, an excitation spectrum can also be recorded. Specifically, we constructed this imaging platform to mitigate the challenges associated with two-dimensional cell culture experiments (*i.e.*, differentiating cell types, determining the electrochemical contribution of each cell type, and distinguishing paracrine from intercellular communication effects[28]).

Detailed User Instructions

Using this platform, three independent measurements may be captured (*i.e.*, an optical, a spectral, and an electrochemical measurement). These data act as members of a set, where each contributes varying useful information. The optical spatial resolution is dependent on the objective lens in use and the diffraction limit of light; generally, a 40x objective lens with 559 nm resolution in the XY plane was used. The wavelength and bandpass resolution are critical to capturing spectral data; a wavelength resolution of 1 nm is feasible if a spectrum is obtained within the bandpass resolution of a single VersaChrome® filter. If a combination of filters must be used to obtain the desired wavelengths within a spectrum, the user is limited by the highest bandpass resolution (*i.e.*, 16 nm) to avoid spectral overlap. Additionally, the spatial resolution of the electrochemical data can be adjusted by varying the size of the electrode tip in use. Furthermore, nanometer spatial resolution, below the diffraction limit of light, can be achieved during electrochemical imaging.[29]

For sample analysis, the components of the system must be turned on in the order denoted by the numbering within **Schematic 1**. Power to the Leica DMi8 inverted microscope and the Leica digital camera are controlled by the Leica CTR advanced electronics box and the SP box. To obtain fluorescence and spectral data *via* variable fluorescence bandpass, wavelengths must be specified using the two Lambda VF-5™ tunable filter changers and the Lambda 10-3 optical filter changer.

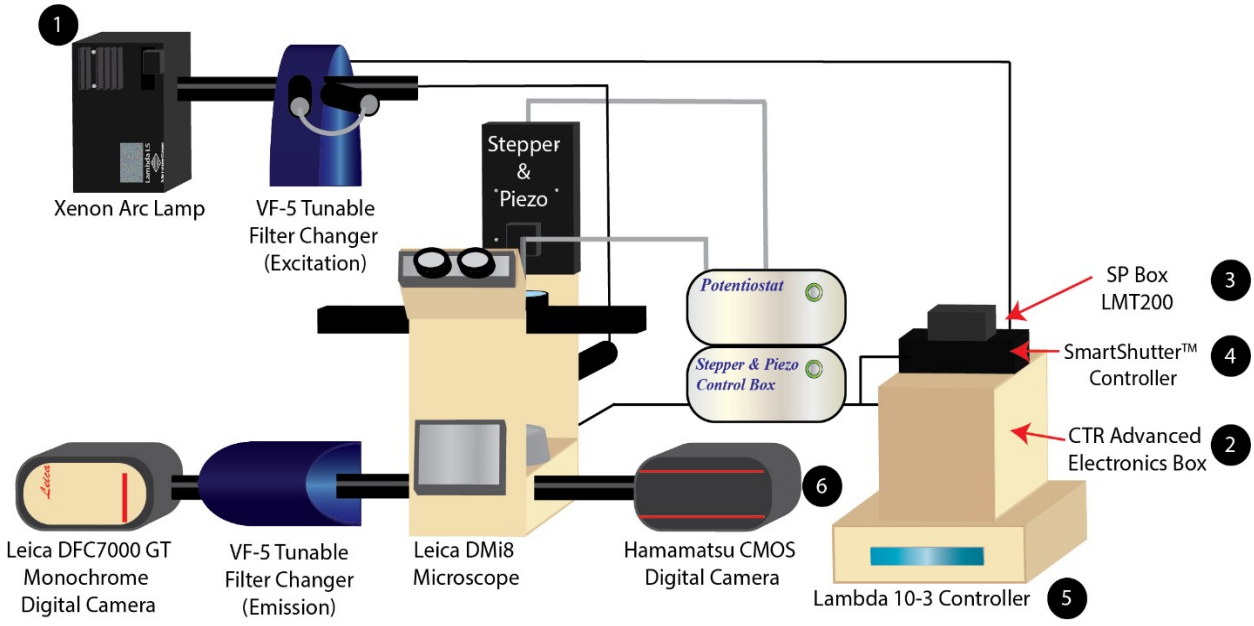

Schematic 1. Schematic of the variable fluorescence bandpass imaging platform with numbered equipment for the power on mechanism.

Initially, the home screen of the Lambda 10-3 displays “A” and “B” wavelength values, “C: OFF”, and “L”. “A” is representative of the emission wavelength and may be programmed using the S1 button, while “B” is representative of the excitation wavelength and may be programmed using the S2 button. “C” and “L” denote functions of the equipment. When “C: OFF” is shown rather than “C: ON” the Lambda *Smart*Shutter™ will not allow light to travel from the xenon illumination source to the excitation tunable filter. One must note that the Lambda *Smart*Shutter™ must be set to “Auto” and “C: ON” must be displayed on the Lambda 10-3 to capture a lambda scan. Additionally, when “Local” is selected on the Lambda 10-3, “L” will be shown on the optical filter changer to initiate local programming. When “On Line” is selected on the Lambda 10-3, “U” will be shown to allow image acquisition *via* the LAS X software based on the local programming of the optical filter changer using a TTL trigger. To use white light to excite typical filter cubes found in the compartment beneath the objective lenses of the Leica DMi8 inverted microscope (*i.e.*, bypass mode or white-light output mode), the Lambda *Smart*Shutter™ must be set to “Open,” “C: ON” must be displayed on the Lambda 10-3, and “B” must be set to 430 nm (*i.e.*, a physically unavailable wavelength based on the current filters in use).

After warming up the xenon arc lamp for 15 minutes, a sample may be placed on the Leica DMi8 stage for analysis. Once the sample is in focus, a bright field image may be obtained using a standard halogen lamp, then fluorescence microscopy images may be obtained in bypass mode using standard filter cubes located in the Leica DMi8 inverted microscope and the Hamamatsu digital camera to the right. Use of this equipment is specified in the Leica LAS X imaging software, and the software is used to capture images. To specify wavelengths to capture fluorescence images, the Lambda 10-3 optical filter changer may be programmed for the excitation and emission of a sample using the following sequence: Local, S1, numerals of the specified emission wavelength, Enter, S2, numerals of the specified excitation wavelength, Enter, Enter, On Line. The corresponding fluorescence image must be obtained using the 80/20 Beam Splitter and the Leica DFC7000 GT digital camera. To obtain the corresponding emission spectrum of the sample, the Lambda 10-3 optical filter changer must be programed to maintain an excitation wavelength of the sample using the technique outlined above. To step through emission wavelengths, the following program should be used: Local, Mode, S1, 4, 1, 1, Enter, numerals of the starting wavelength, Enter, numerals of the ending wavelength, Enter, numerals of the step size, Enter, 1, Enter, 0 (3×), Enter, On Line. One must note, that here the direction of the scan can be set to ascend or descend

depending on the type of spectrum desired. The program detailed here sets the emission wavelengths to scale up. Following entering the program, an asterisk should be displayed to the right of the emission wavelength on the home screen of the controller to denote that the emission wavelength may change according to the previously mentioned program. This allows the use of a TTL trigger based on an emission trigger to step through wavelengths evenly using the Leica LAS X time lapse imaging software. Within the Leica LAS X software, a lambda scan may be initiated after selecting "t" in the upper left corner of the "Acquisition" tab and inputting parameters specific to the imaging system and the specified emission wavelength range. Within the "Project settings" window in the left-hand tool bar, "use sequencer advanced" and "single image mode" must be selected. In this window under "Z-Movement," "Z then Lambda" should be selected and the "Shutter control" should be "optimized." Within the "t" window, the time interval may be adjusted based on the exposure time (for the purpose of imaging microspheres in this manuscript it was set to 10 seconds), the number of pulses (*i.e.*, the number of mechanical spectral shifts) should be set to 1 for a duration (*i.e.*, the amount of time between each mechanical shift limited physically by the filter wheel) of 50 milliseconds, and the cycle number should be based on **Equation 1** (for the purpose of imaging the microspheres in this manuscript it was set to 26).

$$\left(\frac{\lambda_{em} - \lambda_{ex}}{step\ size}\right) + 1 \quad (1)$$

Additionally, within the "Triggering" window, "Emission Trig" must be checked as well as "Use in experiment." The trigger should be linked to the first channel only and occur before the acquisition. To begin the acquisition, "Start" should be selected in the bottom right of the "Acquisition" tab. Following acquisition, within the "Quantify" tab of the software, a stack profile is rendered to produce an emission spectrum that is converted to a Microsoft Excel file for further use.

Cyclic Voltammetry of Ferrocenemethanol

Prior to approaching Hep G2 cells, a cyclic voltammogram was taken at a distance sufficiently away from the insulating tissue culture dish (*i.e.*, where $i_T = i_{T,\infty}$ when $z \geq 10a$, where a is the radius of the electrode) to verify the response of the Pt SECM tip prior to imaging. The limiting current at +0.5 V vs. Ag/AgCl was used to calculate the concentration of ferrocenemethanol based on **Equation 2**, where i_l is the limiting current, n is the number of electrons (n=1), F is Faraday's constant (96485 C/mol), D is the diffusion coefficient of ferrocenemethanol (D= 7.00 × 10^{-6} cm^2/s), and r is the radius of the electrode (r=5 μm).

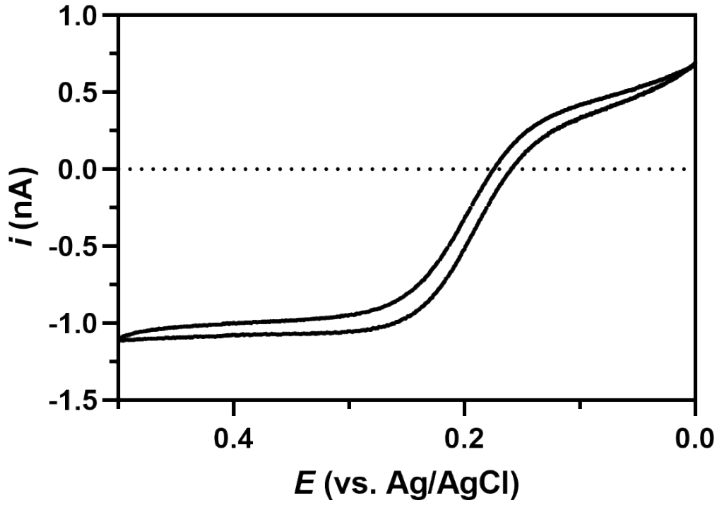

$$i_{(l)} = 4nFDC^{*}r_{(0)} \quad (2)$$

Figure S1. Cyclic voltammogram of 0.80 mM FcMeOH in DPBS (1X) in a 3.5 cm tissue culture dish > 500 μm above Hep G2 cells at a Pt SECM tip (r = 5 μm) vs. Ag/AgCl. A thin glassy carbon rod was used as the counter electrode. This cyclic voltammogram was used to verify the response of the Pt SECM tip prior to collecting the scanning electrochemical microscopy image featured in Figure 5.

Cyclic voltammograms (**Figure S1**) were captured before obtaining each SECM image provided in this manuscript. Variations in faradaic responses due to variation in ferrocenemethanol concentration and changes in RG between electrochemical imaging were normalized by provided normalized current scales for SECM images; additionally, electrochemical images were only used for qualitative analysis.

Following cyclic voltammetry above cells, an approach to cells is completed by holding the Pt SECM tip at +0.5 V vs. Ag/AgCl. The approach is concurrently monitored using bright field microscopy. Once an increase in feedback is observed, indicating the tip is directly above the cell surface (**Figure S2**), the tip is retracted 5 to 10 μm to avoid tip-sample crashing while imaging in constant height mode.

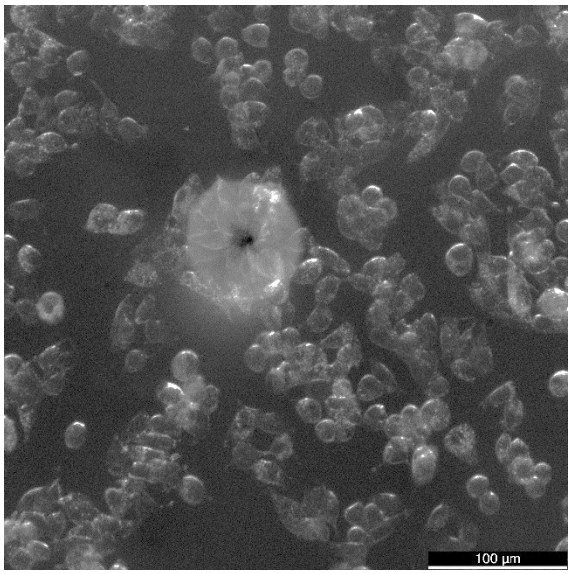

Figure S2. Optical image of Pt SECM tip (r = 5 μm) directly above Hep G2 P27 cell directly after an amperometric approach at +0.5 V vs. Ag/AgCl.

Assessment of Cell Viability of Hep G2 Cells

As shown in **Figure S3**, seemingly viable cells displayed an increase in the feedback response relative to the tissue culture dish within electrochemical images, while others that had assumed a spherical morphology in bright field microscopy (**Figure S3b**) displayed a decrease in the feedback response. It is inferred that the increase in the feedback response of viable cells is due to the bioaccumulation of ferrocenemethanol, followed by the expulsion of reduced glutathione capable of converting ferrocenium methanol back to ferrocenemethanol.[30] Alternatively, the decrease in the feedback response agrees with the onset of apoptotic death due to ferrocenemethanol bioaccumulation as hepatocellular carcinoma cells typically shrink, detach, and become spherical as a result of apoptotic death and loss of cell viability.[31] We hypothesize that the decrease in feedback is observed due to no (or very little) metabolic activity.

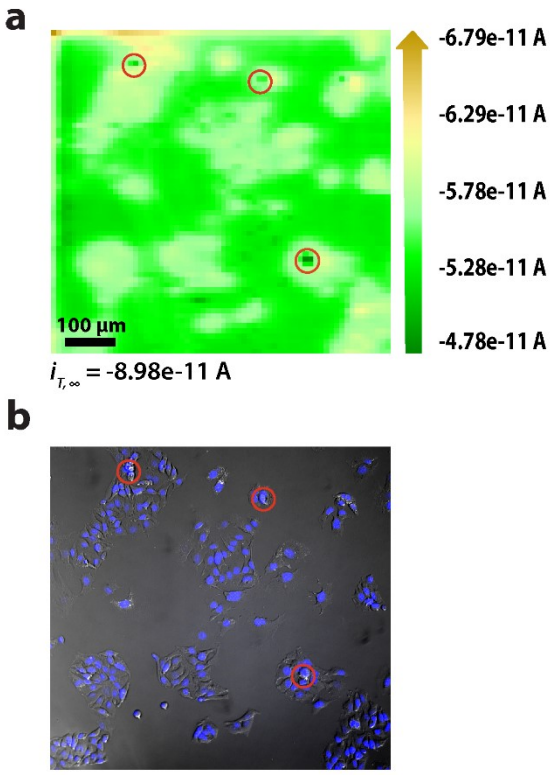

Figure S3. (a) Correlated polarographic electrochemical image and **(b)** bright field/fluorescence overlay of Hep G2 cells. The electrochemical image was obtained with a Pt microelectrode tip (r = 5 µm) vs. Ag/AgCl in ~70 µM ferrocenemethanol in DPBS (1X, pH 7.4). The fluorescence image was false colored for visual representation. Cell nuclei stained with Hoechst 33342 ($\lambda_{ex}/\lambda_{em}$, 400/497 nm). Cells with spherical morphology highlighted in red.

Assessment of Cell Redox Activity of Hep G2 Cells: Spectral Quantification of ROS and Glutathione

Hep G2 cells were cultured in a 3.5 cm poly-L-lysine treated tissue culture dish using DMEM – high glucose supplemented with 10% fetal bovine serum, 2.5% HEPES buffer, and 1% penicillin-streptomycin (*i.e.*, full growth media). Cells were incubated at 37 °C, 5% CO_2, and 10% O_2 until they reached 65 to 85% confluence. Full growth media replaced with 2 mL solution of 10 μM dichlorofluorescein diacetate in DPBS (1X, pH 7.4). Cells incubated at room temperature for 20 minutes, then the solution was replaced with ferrocenemethanol/monochlorobimane in DPBS (1X, pH 7.4) for scanning electrochemical microscopy with complementary hyperspectral imaging. Hyperspectral analysis of ROS and the monochlorobimane/glutathione conjugate was assessed because glutathione production at the cell surface due to oxidative stress induced by ferrocenemethanol has been indicated previously in the literature.[30]

Cells were brought into focus using a standard halogen lamp. A typical fluorescence image was captured using a standard DAPI filter cube and the Hamamatsu digital camera (bypass mode addressed earlier in the Supporting Information) (**Figure S4b**). The variable fluorescence bandpass system was used to capture hyperspectral images; these additional fluorescence images were captured using an 80/20 Beam Splitter and the Leica DFC7000 GT digital camera. To obtain an emission spectrum for dichlorofluorescein (**Figure S4c**), the Lambda 10-3 optical filter changer was programmed to maintain an excitation wavelength of 495 nm and step through emission wavelengths of 535 nm to 550 nm with a step size of 1 nm. To obtain an emission spectrum for monochlorobimane/glutathione (**Figure S4d**), the Lambda 10-3 optical filter changer was programmed to maintain an excitation wavelength of 390 nm and step through emission wavelengths of 470 nm to 500 nm with a step size of 1 nm. A stack profile of the images captured at each emission wavelength was rendered to produce emission spectra of Hep G2 cells. An emission peak for dichlorofluorescein cannot be fully resolved due to spectral overlap of excitation and emission filters in this range. Subsequent electrochemical imaging (**Figure S4a**) was completed as previously described in the main text.

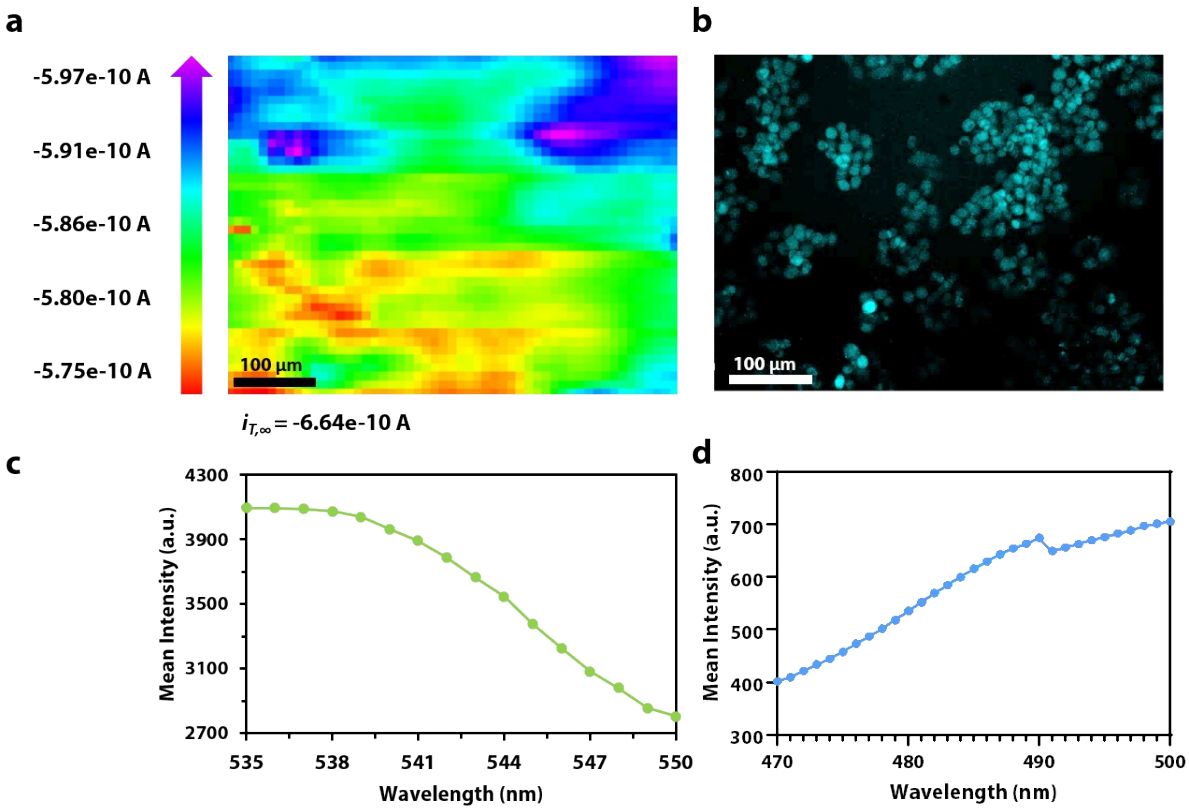

Figure S4. (a) Correlated polarographic electrochemical image and **(b)** fluorescence image of Hep G2 cells. The electrochemical image was obtained with a Pt microelectrode tip (r = 5 µm) vs. Ag/AgCl in 0.50 mM ferrocenemethanol/20 µM monochlorobimane in DPBS (1X, pH 7.4). The fluorescence image was false colored for visual representation of the fluorescence of the monochlorobimane/glutathione conjugate at the cell surface ($\lambda_{ex}/\lambda_{em}$, 390/490 nm). **(c)** Correlated emission spectrum of dichlorofluorescein with 1 nm resolution ($\lambda_{ex}/\lambda_{em}$, 495/535 to 550 nm). **(d)** Correlated emission spectrum of monochlorobimane/glutathione conjugate with 1 nm resolution ($\lambda_{ex}/\lambda_{em}$, 390/470 to 500 nm).

References

1. E. Lubeck and L. Cai, *Nature Methods*, 2012, **9**, 743-U159.
2. H. Liu, Z. J. Ye, X. Wang, L. Wei and L. H. Xiao, *Analyst*, 2019, **144**, 859-871.
3. Q. L. Li, X. F. He, Y. T. Wang, H. Y. Liu, D. R. Xu and F. M. Guo, *Journal of Biomedical Optics*, 2013, **18**.
4. Q. A. Alshammari, R. Pala, N. Katzir and S. M. Nauli, *Scientific Reports*, 2021, **11**.
5. M. H. Sung and J. G. McNally, *Wiley Interdisciplinary Reviews-Systems Biology and Medicine*, 2011, **3**, 167-182.
6. M. S. Cohen, M. L. Stewart, R. H. Goodman and X. A. Cambronne, *Adp-Ribosylation and Nad+ Utilizing Enzymes: Methods and Protocols*, 2018, **1813**, 391-414.
7. T. Zimmermann, J. Rietdorf and R. Pepperkok, *Febs Letters*, 2003, **546**, 87-92.
8. H. Matsuoka, Y. Kosai, M. Saito, N. Takeyama and H. Suto, *Journal of Biotechnology*, 2002, **94**, 299-308.
9. K. Asai, Y. Sumiyama, M. Watanabe and K. Aizawa, *Surgery Today*, 2006, **36**, 1075-1084.
10. S. J. Leavesley, M. Walters, C. Lopez, T. Baker, P. F. Favreau, T. C. Rich, P. F. Rider and C. W. Boudreaux, *Journal of Biomedical Optics*, 2016, **21**, 10.
11. J. Moreau, P. Bouzy, J. Guillard, V. Untereiner, R. Garnotel, A. Marchal, C. Gobinet, C. Terryn, G. D. Sockalingum and G. Thiefin, *Molecules*, 2020, **25**.
12. G. Thomas, J. van Voskuilen, H. Truong, J. Y. Song, H. C. Gerritsen and H. Sterenborg, *Biomedical Optics Express*, 2014, **5**, 4281-4299.
13. A. Travo, O. Piot, R. Wolthuis, C. Gobinet, M. Manfait, J. Bara, M. E. Forgue-Lafitte and P. Jeannesson, *Histopathology*, 2010, **56**, 921-931.
14. A. Dvornikov and E. Gratton, *Biomedical Optics Express*, 2018, **9**.
15. M. Ghaffari, A. L. Chateigner-Boutin, F. Guillon, M. F. Devaux, H. Abdollahi and L. Duponchel, *Analytica Chimica Acta*, 2019, **1062**, 47-59.
16. B. R. Masters and P. T. C. So, *Optics Express*, 2001, **8**, 2-10.
17. E. C. Jensen, *Anatomical Record-Advances in Integrative Anatomy and Evolutionary Biology*, 2013, **296**, 1-8.
18. K. Bahlmann, S. Jakobs and S. W. Hell, *Ultramicroscopy*, 2001, **87**, 155-164.
19. C. P. Byers, B. S. Hoener, W. S. Chang, M. Yorulmaz, S. Link and C. F. Landes, *Journal of Physical Chemistry B*, 2014, **118**, 14047-14055.
20. K. Lindfors, T. Kalkbrenner, P. Stoller and V. Sandoghdar, *Physical Review Letters*, 2004, **93**, 4.
21. P. Saha, J. W. Hill, J. D. Walmsley and C. M. Hill, *Analytical Chemistry*, 2018, **90**, 12832-12839.
22. S. R. Kirchner, K. W. Smith, B. S. Hoener, S. S. E. Collins, W. X. Wang, Y. Y. Cai, C. Kinnear, H. Y. Zhang, W. S. Chang, P. Mulvaney, C. F. Landes and S. Link, *Journal of Physical Chemistry C*, 2018, **122**, 6865-6875.
23. J. Juan-Colas, I. S. Hitchcock, M. Coles, S. Johnson and T. F. Krauss, *Proceedings of the National Academy of Sciences of the United States of America*, 2018, **115**, 13204-13209.
24. K. Wonner, M. V. Evers and K. Tschulik, *Journal of the American Chemical Society*, 2018, **140**, 12658-12661.
25. Y. Nomura, K. Yamamoto, T. Hirayama, M. Ohkawa, E. Igaki, N. Hojo and K. Saitoh, *Nano Letters*, 2018, **18**, 5892-5898.
26. P. F. Favreau, C. Hernandez, T. Heaster, D. F. Alvarez, T. C. Rich, P. Prabhat and S. J. Leavesley, *Journal of Biomedical Optics*, 2014, **19**, 10.
27. B. D. B. Aaronson, J. C. Byers, A. W. Colburn, K. McKelvey and P. R. Unwin, *Analytical Chemistry*, 2015, **87**, 4129-4133.

28. K. G. Battiston, J. W. C. Cheung, D. Jain and J. P. Santerre, *Biomaterials*, 2014, **35**, 4465-4476.
29. B. B. Katemann, A. Schulte and W. Schuhmann, *Electroanalysis*, 2004, **16**, 60-65.
30. S. Kuss, R. Cornut, I. Beaulieu, M. A. Mezour, B. Annabi and J. Mauzeroll, *Bioelectrochemistry*, 2011, **82**, 29-37.
31. Y. R. Liao, C. C. Lu, K. C. Lai, J. S. Yang, S. C. Kuo, Y. F. Wen, S. Fushiya and T. S. Wu, *Molecular Medicine Reports*, 2013, **7**, 1539-1544.